The value of [B], the total base concentration, is found to be 9.0×10^{-6}, or pH = 9.1. This corresponds to a catalytic rate constant of 31×10^{-8} s^{-1} at 25 °C, or 4 times larger than the 7.1×10^{-8} s^{-1} calculated at pH 8.6.

Thus only a modest improvement in catalytic efficiency can be hoped for by optimizing conditions. $Fe(CO)_5$ is a poor catalyst because the two steps involved in the catalytic cycle have exactly opposite pH requirements. It may be noted that $Fe(CO)_5$ is not a catalyst for the WGSR in acid media,[31] as expected from our results.

Acknowledgment. This work was supported by the National Science Foundation, Grant No. CH-77-24717.

(31) Ford, P. C.; Ungermann, C.; Landis, V.; Moya, S.; Rinker, R. G.; Laine, R. M., *Adv. Chem. Ser.* **1979**, *No. 173*, 81.

Bistability and Oscillations in the Autocatalytic Chlorite–Iodide Reaction in a Stirred-Flow Reactor[1]

Christopher E. Dateo, Miklós Orbán,[2] Patrick De Kepper,[3] and Irving R. Epstein*

Contribution from the Department of Chemistry, Brandeis University, Waltham, Massachusetts 02254. *Received July 14, 1981*

Abstract: The reaction between chlorite and iodide in acidic solution ($0.08 < pH < 3.75$) has been studied in a stirred-tank reactor at 25 °C over a range of flow rates, pH, and input chlorite and iodide concentrations. The system is found to exhibit bistability and, at high $[ClO_2^-]$ and $[I^-]$, sustained oscillations as well. The key reaction which gives rise to these phenomena is $ClO_2^- + 4I^- + 4H^+ = Cl^- + 2I_2 + 2H_2O$, which is autocatalytic in iodine and is inhibited by iodide. The existence of bistability and oscillations in this system is consistent with the "cross-shaped phase diagram" model of Boissonade and De Kepper.

The recent report of the first systematically designed homogeneous chemical oscillator[4] emphasizes the enormous amount that may be learned about the dynamics of complex chemical systems from the study of autocatalytic reactions in a continuous-flow stirred-tank reactor (CSTR). In the above mentioned study, two autocatalytic subsystems, arsenite–iodate and chlorite–iodide, were linked together in a CSTR to give rise to oscillation. The existence of sustained oscillation in that system had been suggested by a model analysis which implied that addition of an appropriate feedback reaction to a system which exhibits bistability in a CSTR should lead to a "cross-shaped phase diagram"[5] in which oscillations appear for a range of input reactant concentrations.

The arsenite–iodate reaction has been thoroughly examined in a CSTR[6,7] and has been found to exhibit bistability under a wide range of conditions. A simple model involving several overall component processes[6] has been shown to give excellent agreement with the experimental observations. Continuing our study of autocatalytic reactions in the CSTR, we report here on the remarkable richness of dynamic behavior exhibited in a flow reactor by the autocatalytic reaction between chlorite and iodide. We have observed not only the expected bistability but also sustained oscillation; the chlorite–iodide system itself is characterized by a "cross-shaped phase diagram". In addition, as we report elsewhere, this reaction forms the basis of an entire new family of oscillating reactions when chlorite- and iodine- containing species (IO_3^-, I^-, or I_2) are combined with a wide variety of reducing[1,4] or oxidizing[8] agents.

(1) Part 5 in the series Systematic Design of Chemical Oscillators. Part 4: Orbán, M.; De Kepper, P.; Epstein, I. R.; Kustin, K. *Nature (London)* **1981**, *292*, 816–818.

(2) Institute of Inorganic and Analytical Chemistry, L. Eötvös University, H-1443, Budapest, Hungary.

(3) Centre de Recherche Paul Pascal, Domaine Universitaire, 33405 Talence, France.

(4) De Kepper, P.; Epstein, I. R.; Kustin, K. *J. Am. Chem. Soc.* **1981**, *103*, 2133–2134. (Part 2).

(5) Boissonade, J.; De Kepper, P. *J. Phys. Chem.* **1980**, *84*, 501–506.

(6) De Kepper, P. Epstein, I. R.; Kustin, K. *J. Am. Chem. Soc.* **1981**, *103*, 6121–6127. (Part 3).

(7) Papsin, G.; Hanna, A.; Showalter, K. *J. Phys. Chem.* **1981**, *85*, 2575–2582.

Experimental Section

The apparatus employed consists of a thermally regulated stirred tank glass (Pyrex) flow reactor, which has been described in detail elsewhere.[6,9] Potentiometric measurements could be made by using either an Orion iodide-specific electrode or a platinum redox electrode with a $Hg/Hg_2SO_4/K_2SO_4$ electrode as reference. Simultaneous measurement of the absorbance of the solution in the CSTR could also be made. Absorbances were generally monitored at 460 nm, the wavelength at which the I_2 extinction coefficient is a maximum. The path length through the cell was 3.5 cm.

The constraints which are at the disposal of the experimenter are the temperature, which was maintained at 25.0 ± 0.1 °C in this series of experiments, the residence time τ (or flow rate $k_0 = 1/\tau$), and the concentrations $[A_i]_0$ that the input species A_i would reach in the reactor if no reaction were to occur. The input chemical species of importance in these experiments are $[ClO_2^-]_0$, $[I^-]_0$, and $[H^+]_0$. Chorite and iodide solutions were prepared by using doubly distilled water from the highest purity commercially available grades of $NaClO_2$ and KI. Reagent solutions were stored in three separate reservoirs. One contained the chorite, stabilized by 0.001 M sodium hydroxide. The iodide solution was prepared in either sodium acetate or sodium sulfate, and the third reservoir contained the corresponding acid, acetic or sulfuric, depending on the pH desired. Thus when the solutions were mixed in the reactor, an acetic acid–acetate or sulfate–bisulfate buffer of the appropriate pH was generated in situ. The pH was measured directly in the output flow.

The Chlorite–Iodide Reaction in Batch

When solutions of chlorite and iodide are mixed in the absence of flow (bath conditions), an initial slow increase in iodine absorbance soon gives way to a rapid exponential rise. If chlorite is in excess, this rise terminates in an abrupt drop-off, with the disappearance of all trace of iodine color. The iodide concentration is found to decrease slowly at first and then to fall suddenly by more than 5 orders of magnitude at about the time of the peak in I_2 absorbance. This behavior is illustrated for a slight stoichiometric excess of chlorite in Figure 1. With still greater excesses, the absorbance drops to and remains at an essentially zero value.

(8) Dateo, C.; Orbán, M.; De Kepper, P.; Epstein, I. R., to be submitted for publication.

(9) Pacault, A.; De Kepper, P.; Hanusse, P.; Rossi, A. *C. R. Heb. Seances Acad. Sci.* **1975**, *281C*, 215–220.

0002-7863/82/1504-0504$01.25/0

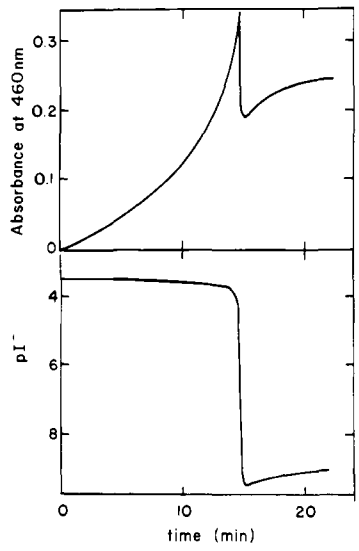

Figure 1. Absorbance at 460 nm and iodide concentration for a batch reaction at 25 °C and pH 3.3 with initial concentrations $[I^-]_i = 4 \times 10^{-4}$ M, $[ClO_2^-]_i = 2.5 \times 10^{-4}$ M.

First studied qualitatively by Bray[10] some 75 years ago, this spectacular clock reaction has been thoroughly investigated in batch by Kern and Kim[11] and by de Meeus and Sigalla.[12]

The initial phase of the reaction is characterized by the stoichiometry of process A. In the presence of excess chlorite, the

$$ClO_2^- + 4I^- + 4H^+ = Cl^- + 2I_2 + 2H_2O \qquad (A)$$

iodine is oxidized further to iodate in process B. If iodide and

$$5ClO_2^- + 2I_2 + 2H_2O = 5Cl^- + 4IO_3^- + 4H^+ \qquad (B)$$

iodate are present simultaneously, then process C is also of significance. The net reaction in the presence of excess chlorite is

$$IO_3^- + 5I^- + 6H^+ = 3I_2 + 3H_2O \qquad (C)$$

(R) = $^1/_2$[(A) + (B)].

$$3ClO_2^- + 2I^- = 2IO_3^- + 3Cl^- \qquad (R)$$

Kinetic studies [11,12] have established that reaction A is autocatalytic in I_2 and is inhibited by I^-, with a rate law of the form[13]

$$\frac{d[I_2]}{dt} = k_{A_1}[H^+][I^-] + k_{A_2}[I_2] + k_{A_3}\frac{[I_2]}{[I^-]} \qquad (1)$$

Reaction B is known to be quite rapid, but a rate law for this process has not yet been established. Process C is the venerable Dushman reaction,[14] the kinetics of which have been studied by numerous workers with a variety of somewhat conflicting results,[15] though a rate law of the form

$$-\frac{d[IO_3^-]}{dt} = k_{C_1}[H^+]^2[IO_3^-][I^-] + k_{C_2}[H^+]^2[IO_3^-][I^-]^2 \qquad (2)$$

seems to have a great deal of evidence in its favor.

The Chlorite–Iodide Reaction in the CSTR

Bistability. Under batch conditions, the final equilibrium state attained by a mixture with the initial composition shown in Figure 1 is uniquely defined. However, as we see in Figure 2, a system with the same initial composition flowed into the CSTR will ultimately be found in either of two quite different stable steady states. The system is said to be bistable.

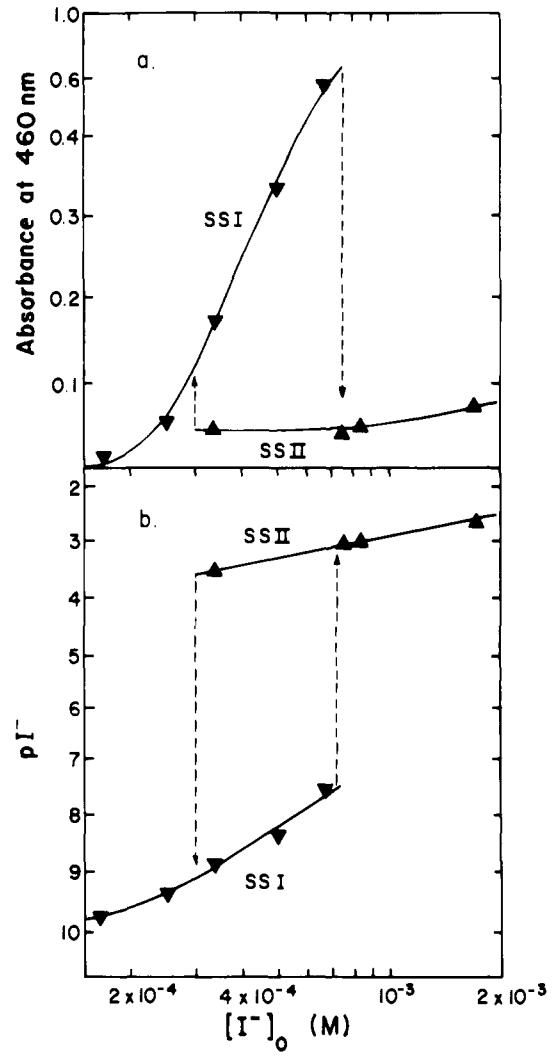

Figure 2. Steady state hysteresis phenomena in the absorbance at 460 nm and the iodide concentration in the CSTR as a function of $[I^-]_0$, with $[ClO_2^-]_0 = 2.5 \times 10^{-4}$ M, pH 3.35, $k_0 = 5.4 \times 10^{-3}$ s^{-1}, and $T = 25$ °C. Dashed arrows indicate spontaneous transitions between states.

Figure 2 shows the steady-state values of the absorbance at 460 nm and of pI^- as functions of the input iodide flow $[I^-]_0$, with all other constraints held constant. At low iodide flow, the system possesses only a single low iodide steady state, designated SSI. This state is an extension of the so-called thermodynamic branch, the set of states which tend continuously toward the equilibrium state as the flow rate approaches zero.

If $[I^-]_0$ is gradually increased, the system remains in SSI until $[I^-]_0$ reaches 6.7×10^{-4} M. A futher increase to $[I^-]_0 = 7.5 \times 10^{-4}$ M induces a transition to a high iodide steady state, denoted SSII. This state, which is the only stable one at higher iodide flows, is the continuation of the flow branch, along which species concentrations are determined primarily by the input flow because the chemical processes are slow relative to the flow. If the iodide flow is now decreased, the system follows the SSII branch as far as $[I^-]_0 = 3.3 \times 10^{-4}$ M. When $[I^-]_0$ is decreased still further to 2.5×10^{-4} M, the iodide concentration in the reactor is observed to drop by a factor exceeding 10^4, bringing the system back to SSI.

The system thus exhibits hysteresis in the transitions from SSI to SSII and back. The region between the two critical transition values of $[I^-]_0$ is a bistable region. In such a region, which state, SSI or SSII, will ultimately be attained by the system depends

(10) Bray, W. C. *Z. Phys. Chem.* **1906**, *54*, 731–749.
(11) Kern, D. M.; Kim, C.-H. *J. Am. Chem. Soc.* **1965**, *87*, 5309–5313.
(12) De Meeus, J.; Sigalla, J. *J. Chim. Phys. Phys.-Chim. Biol.* **1966**, *63*, 453–459.
(13) The absence of the K_{A_2} term in the rate law reported in ref 11 is compatible with the values of the rate constants given in ref 11 and 12 and with the much higher iodide concentrations employed in the experiments of ref 12.
(14) Dushman, S. J. *J. Phys. Chem.* **1904**, *8*, 453–482.
(15) Liebhafsky, H. A.; Roe, G. M. *Int. J. Chem. Kinet.* **1979**, *11*, 693–703.

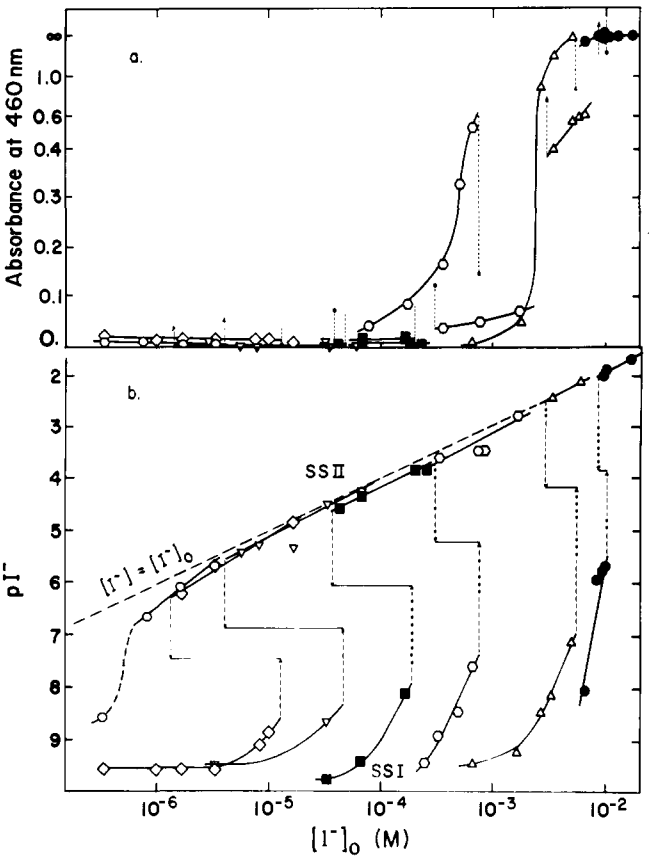

Figure 3. As in Figure 2, but for a series of $[ClO_2^-]_0$ values: ○, 10^{-6} M; ◇, 3.3×10^{-6} M; ▽, 10^{-5} M; ■, 5×10^{-5} M; ○, 2.5×10^{-4} M; △, 2.5×10^{-3} M, ●, 6.7×10^{-3} M. Thin horizontal lines show width of the hysteresis loop.

upon how the actual values of the constraints are reached; i.e., whether the iodide flow is adjusted to $[I^-]_0$ from above or from below.

The experiment described above can be repeated for a range of input chlorite concentration, enabling us to observe how the $[I^-]_0$ hysteresis loop evolves as a function of $[ClO_2^-]_0$. As we see in Figure 3, the width of the bistable region increases with decreasing $[ClO_2^-]_0$ until $[ClO_2^-]_0 = 3.3 \times 10^{-6}$ M. At a critical $[ClO_2^-]_0$ value, bistability suddenly disappears, and, as shown for $[ClO_2^-]_0 = 1.0 \times 10^{-6}$ M, the distinction between SSI and SSII vanishes as $[I^-]_{SS}$ changes continuously with increasing $[I^-]_0$.

At the other end of the range of chlorite flows, the width of the hysteresis loop decreases with increasing $[ClO_2^-]_0$, though the iodide concentrations in the two states still differ by a factor of 10^4 or more. We were unable to observe the system at $[ClO_2^-]_0$ flows above 6.7×10^{-3} M because of interference from solid iodine which precipitates under those conditions. Notice that, except at the lowest values of $[I^-]_0$ and $[ClO_2^-]_0$, the iodide concentration in SSII follows that in the flow almost exactly.

The absorbance, which is shown in Figure 3, proved to be a less generally informative monitor of the system than did the potential of the iodide-sensitive electrode. For $[ClO_2^-]_0 \leq 5 \times 10^{-5}$ M no measurable absorbance was found, while for $[ClO_2^-]_0 \geq 6.7 \times 10^{-3}$ M the solutions were so dark that no difference in absorbance between SSI and SSII could be observed.

In Figure 4, we show the extent of the bistable region in the $[ClO_2^-]_0$–$[I^-]_0$ plane with the other constraints held fixed. This figure summarizes the results presented in Figure 3 and constitutes a two-dimensional section of the full multidimensional phase diagram of the system.

If we fix the chlorite input flow and vary the pH and $[I^-]_0$, we obtain another bistability region and hysteresis phenomenon as shown in Figures 5 and 6. Although, as Figure 5 demonstrates, the width of the bistable region shrinks as the pH is decreased, the relative difference in $[I^-]_{SS}$ between the two steady states

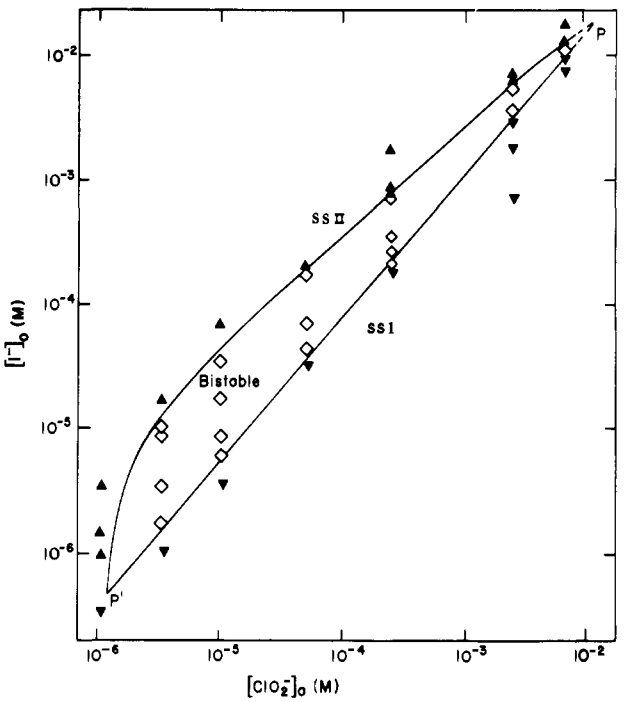

Figure 4. A section of the phase diagram in the $[ClO_2^-]_0$–$[I^-]_0$ plane with all other constraints as in Figure 2: ▼, SSI; ▲, SSII; ◇, bistability SSI/SSII. P and P' indicate the cross points or critical points where the bistable region disappears as SSI and SSII coalesce. P cannot be observed directly under these conditions because of iodine precipitation in the region indicated by dashed lines.

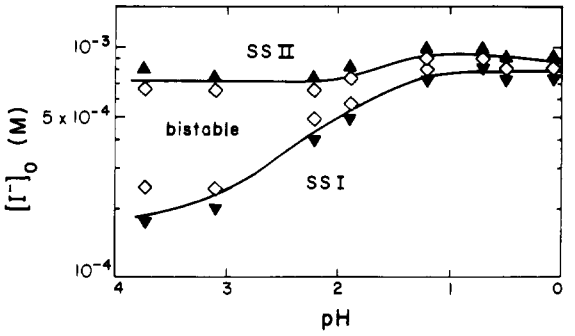

Figure 5. A section of the phase diagram in the $[I^-]_0$–pH plane showing bistability with all other constraints as in Figure 2. Symbols are as in Figure 4.

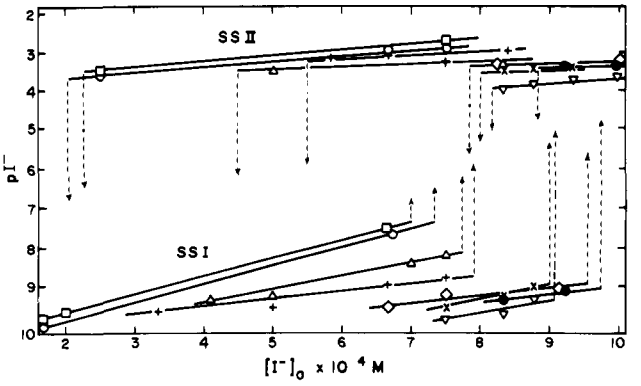

Figure 6. Steady-state iodide concentrations vs. $[I^-]_0$ for the conditions shown in Figure 5, illustrating the hysteresis phenomenon. Dashed arrows indicate spontaneous transitions between states for a series of pH values: ○, 3.75; □, 3.10; △, 2.20; +, 1.93; ◇, 1.20; ●, 0.70; X, 0.50; ▽, 0.08.

remains constant or even increases slightly at low pH, as illustrated in Figure 6. Because of the strong dependence of the potential

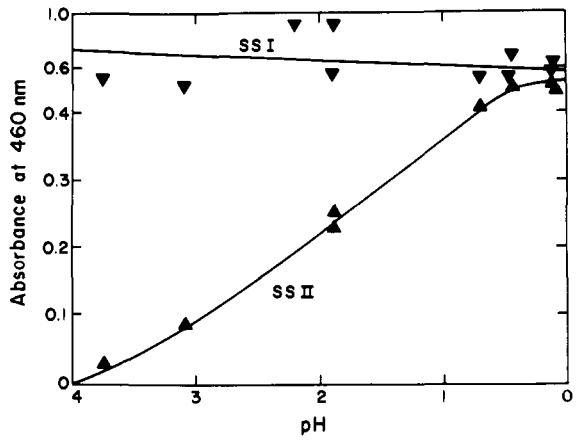

Figure 7. Absorbance at 460 nm vs. pH with $[ClO_2^-]_0 = 2.5 \times 10^{-4}$ M, $[I^-]_0 = (7.5 \pm 0.8) \times 10^{-4}$ M, $k_0 = 5.4 \times 10^{-3}$ s^{-1}, and $T = 25$ °C: ▼, SSI; ▲, SSII.

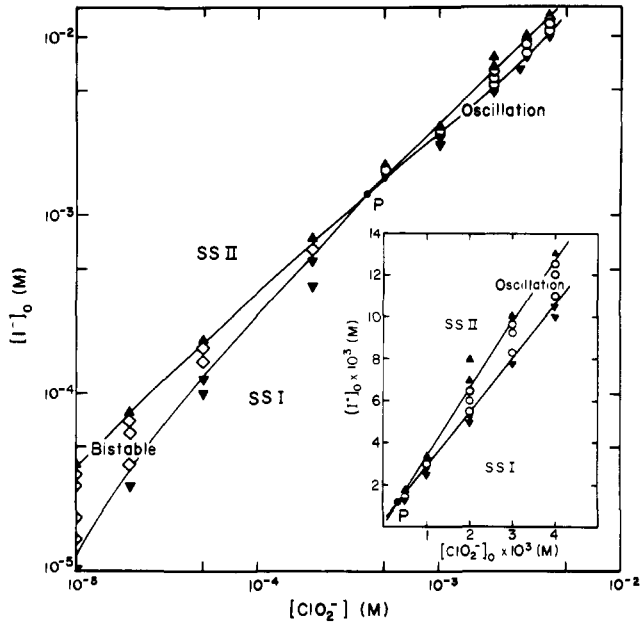

Figure 8. Log-log plot of a section of the phase diagram in the $[ClO_2^-]_0$–$[I^-]_0$ plane with pH 2.04, $k_0 = 1.1 \times 10^{-3}$ s^{-1}, and $T = 25$ °C: ▲, SSI; ▼, SSII; ◇, bistable; ○, oscillatory. Inset shows the same data on a linear scale. *P* indicates cross point.

of the iodide-sensitive electrode on pH, the pI^- values in Figure 6 have been calibrated at several different pHs. Measurements could not be made at pH values significantly below 0.08 because the input tube would deteriorate under such acidic conditions.

Figure 7 shows the variation of the optical densities of SSI and SSII with pH. While the optical density of SSI is nearly independent of pH, that of SSII increases dramatically with the acidity of the solution. A noticeable odor of ClO_2 appeared at low pH, which is consistent with the known increase in decomposition of chlorite at higher acidity.[16]

Oscillation. Another section of the phase diagram in the $[ClO_2^-]_0$–$[I^-]_0$ plane is shown in Figure 8 for a lower pH and longer residence time than employed in Figure 4. By changing the experimental constraints in this manner, we have shifted the critical point *P* in Figures 4 and 8 to lower $[ClO_2^-]_0$ and $[I^-]_0$. As a result of this shift, we are now able to observe, without the problem of iodine precipitation, the portion of the phase diagram at high $[ClO_2^-]_0$ and $[I^-]_0$ above the bistable region.

A new and exciting feature now emerges. There is a region in which the system oscillates! This oscillatory region is seen more clearly on the insert in Figure 8, where the phase diagram is redrawn with a linear scale. Near the cross point, very long (about 30 min) period oscillations are observed, and the $[I^-]$ amplitude of the oscillations is quite close to the difference in iodide concentration between SSI and SSII in the neighboring bistable region.

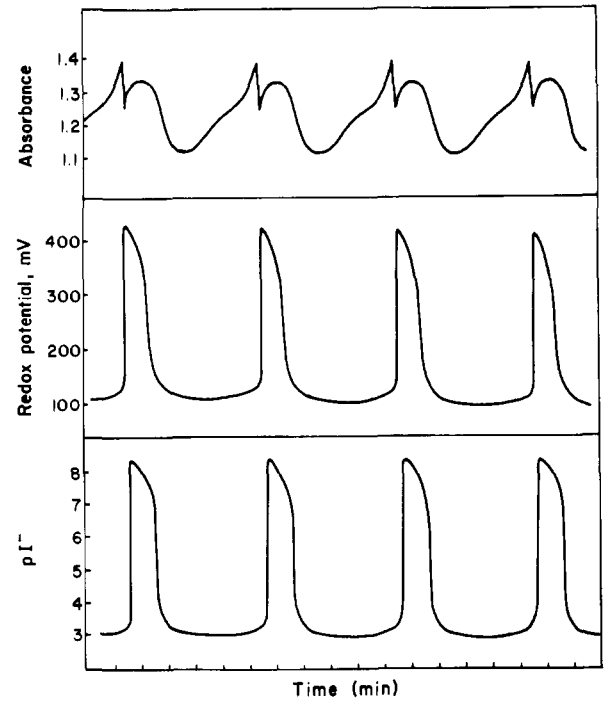

Figure 9. Oscillations in the absorbance at 460 nm, iodide concentration, and potential of a platinum redox electrode (vs. $Hg|Hg_2SO_4||K_2SO_4$ reference electrode) with time.

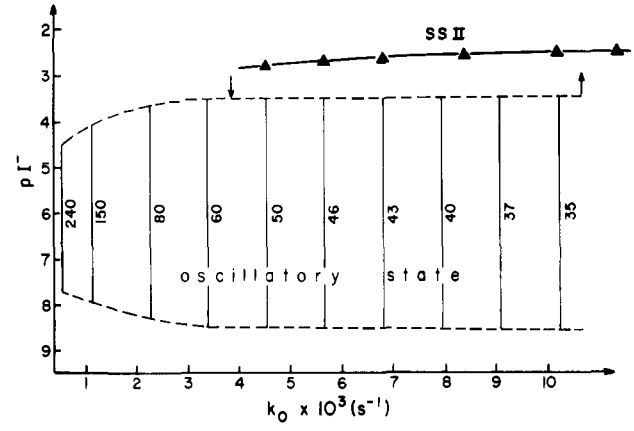

Figure 10. Hysteresis in the transition between SSII and the oscillatory state as a function of flow rate k_0 with $[I^-]_0 = 0.0065$ M, $[ClO_2^-]_0 = 0.002$ M, pH 1.56, and $T = 25$ C. Envelopes of vertical segments show upper and lower limits of pI^- in the oscillatory state. Numbers next to these segments indicate period of oscillation in seconds. Arrows indicate spontaneous transitions between states.

In Figure 9 we show typical oscillatory traces of the absorbance, Pt redox electrode potential, and iodide specific electrode potential for a composition in this region. The period of the oscillations generally decreases with increasing $[ClO_2^-]_0$ and $[I^-]_0$ and k_0.

The period and amplitude of the oscillations also decrease as $[H^+]_0$ is increased. At pH values below 2 we observe in addition a new hysteresis phenomenon in the transition between the oscillatory state and SSII. This type of hysteresis is illustrated in Figure 10 as a function of the flow rate $k_0 = 1/\tau$. Starting at low k_0, the system resides in the oscillatory state. As the flow rate is increased, oscillations persist with slightly increasing amplitude and decreasing period until $k_0 = 10.2 \times 10^{-3}$ s^{-1}. When the flow rate is further increased to 11.3×10^{-3} s^{-1}, full amplitude

(16) Gordon, G.; Kieffer, R. G.; Rosenbaltt, D. H. *Prog. Inorg. Chem.* **1972**, *15*, 201–286.

oscillations suddenly vanish, giving way to the high iodide non-oscillatory SSII as the only stable state of the system. If the flow rate is now decreased, the system remains in SSII until $k_0 = 3.7 \times 10^{-3}$ s^{-1}, where a sudden drop in the [I$^-$] level in the reaction mixture brings the system abruptly back into the oscillating state. At low pH, then, we have a rather broad region of bistability as a function of flow rate between steady-state SSII and an oscillatory state.

Discussion

Although the responses measured in these experiments, absorbance at 460 nm and potentials of the platinum- and iodide-specific electrodes, provide a clear picture of the behavior of the system with respect to bistability, oscillation, and hysteresis phenomena, there are some ambiguities in relating the measured quantities directly to concentrations of species in the reactor.

While 460 nm was selected as the wavelength of maximum absorbance ($\epsilon^{460} = 770$) of I_2, at least two other species, I_3^- ($\epsilon^{460} = 780$) and ClO_2 ($\epsilon^{460} = 32$) also absorb significantly in this region. The triiodide contribution can be expected to be of importance as a result of the rapid equilibrium

$$I_2 + I^- = I_3^- \qquad K_{eq} = 830\ M^{-1}$$

when [I$^-$] in the reactor exceeds 10^{-4} M. Chlorine dioxide formation appears to be significant at high input chlorite concentrations, especially at very low pH. Under these conditions, the odor of ClO_2 was easily detectable. These multiple contributions to the absorbance may account for absorbance traces such as that of Figure 9, in which each period of oscillation shows two or more peaks while the corresponding potential trace contains only a single maximum.

Some lack of reproducibility was found in the potential of the iodide-specific electrode at low pH and high [I_2], even when no iodine precipitation was observed. In these regions, the platinum electrode appears to perform more reliably, though whether it responds exclusively to the I^-/I_2 couple under these conditions is unclear.

In Figures 4 and 8, the line which divides the bistable or the oscillatory region from the high iodide state SSII corresponds to a ratio of $[I^-]_0$ to $[ClO_2^-]_0$ of approximately 4. This observation suggests, since the I^-/ClO_2^- ratios of reactions A and R are 4 and 2/3, respectively, that the autocatalytic process A is the key step in controlling the bistability, while processes B and/or C may provide the feedback necessary to bring about oscillation.

While we have not attempted to formulate a detailed mechanism to account for the observed phenomena, we believe that some general conclusions can be drawn about the underlying dynamics of this system. The phase diagram of Figure 8, in which an oscillatory and a bistable region join at the intersection of the stability boundaries of two steady states, is the characteristic "cross-shaped" diagram described by Boissonade and De Kepper,[5] in which an intrinsically bistable subsystem (process A) is associated with a slower feedback reaction. Since the feedback process must have a slower time scale than the reaction which determines the bistability,[5] process C would appear to be the rate-determining step in the feedback sequence, given that (B) is known to be extremely rapid.

In this study we have measured the time dependence of certain system responses such as [I$^-$] or absorbance at 460 nm as functions of the constraints. In principle, with sufficient data of this sort, one could eliminate time as a variable and, for given values of the other constraints, construct the trajectories which describe the dynamic behavior of the system. These trajectories could then be combined into a phase portrait which would show the topological structure of the system dynamics. For example, this sort of analysis would allow us to distinguish between two plausible topological configurations (Figure 11) which might account for the hysteresis phenomenon shown in Figure 10. We now examine these topological situations in turn and show how the experimental results permit us to eliminate one in favor of the other.

The evolution of these two topological cases is shown in Figure 11 as a function of the flow rate k_0. Case A corresponds to a

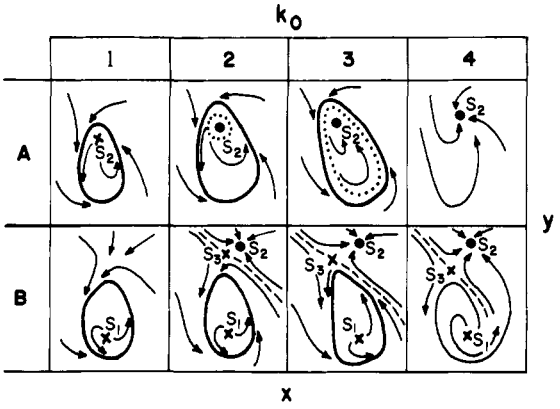

Figure 11. Possible topological configurations for the hysteresis phenomenon of Figure 10 (see text): ●, stable steady state; ×, unstable steady state; O, stable limit cycle; ⋮, unstable limit cycle; - - -, separatrix. In each scheme (A, B), each block (1–4) represents a sketch of the X–Y response plane, while k_0 increases as we move across the flow chart from block 1 to block 4. X and Y might represent [I^-] and absorbance at 460 nm.

subcritical Hopf bifurcation,[17] in which a stable steady state, an unstable limit cycle, and a stable limit cycle interact to give the hysteresis loop. In case B, three stationary states, two of which are unstable, a separatrix, and a stable limit cycle come into play. We now describe the system behavior in each case as k_0 is varied starting from high values of k_0 in block 4.

In case A, the system starts in S_2 and remains in that state through blocks 3 and 2 in which a stable cycle and an unstable limit cycle appear and diverge from one another. Finally, as k_0 is decreased beyond block 2, the unstable limit cycle continues to shrink until it collides with S_2, which then becomes unstable as the limit cycle disappears. Beyond this point, as in block 1, the system is left with only one stable solution, the limit cycle. We have a hard transition from the steady-state S_2 to the oscillatory state. If we now reverse the process and increase k_0, the system remains on this periodic solution through blocks 2 and 3 until finally the stable and unstable limit cycles fuse, annihilating one another and forcing a hard transition into the only remaining stable state S_2, as in block 4. The behavior described above is mirrored by the hysteresis in the transitions between oscillatory and stationary states seen in Figure 10.

In the alternative case B, the system is also found in steady-state S_2 at high values of k_0 (block 4). As k_0 is decreased, a stable limit cycle develops around the unstable state S_1 and the separatrix divides the set of system trajectories into two disjoint sets, those which evolve to S_2 and those which tend toward the limit cycle about S_1. When k_0 is decreased still further, the stable steady-state S_2 and the saddle point S_3 approach one another until they fuse and vanish forcing the system into the unique stable periodic solution surrounding S_1 (block 1). If we now reverse direction and increase k_0, the system remains on the lower side of the separatrix on the limit cycle until, with increasing k_0, the limit cycle grows to the point where it collides with the separatrix and vanishes, inducing a transition back to S_2 as in block 4. It is of crucial importance here that as the limit cycle approaches the separatrix, it must also approach the saddle point S_3, causing the period of the oscillations to diverge, since at S_3 we must have $dx_i/dt = 0$.

This expected increase in oscillation period with increasing k_0 is not consistent with the behavior seen in Figure 10, where the period decreases with the flow rate. Thus topology A appears to be the most likely one for our system. The fact that the [I$^-$] values in the steady state of Figure 10 lie outside the range of [I$^-$] in the oscillatory state can be reconciled with the existence of S_2 inside the limit cycle of Figure 11 by observing that the topological sketches are drawn for a two-dimensional system while

(17) Marsden, J.; McCracken, M. "The Hopf Bifurcation and its Applications"; Springer-Verlag: New York, 1976.

the actual dimensionality of our system is almost certainly greater than 2.

Our choice of topology A is reinforced by the fact that the oscillations of Figure 10 connect directly to those observed in the neighborhood of the cross point P in Figure 8. From the cross-shaped diagram theory,[5] such oscillations result from periodic transitions between two steady states, which cannot occur in case B where the oscillations are an intrinsic property only of the low iodide branch corresponding to the S_1 state. The theory predicts that oscillating systems resulting from the combination of bistability and a feedback can easily give rise to a subcritical bifurcation as in A and that as the time scale of the feedback decreases, resulting in a shorter oscillation period, the width of the hysteresis region will initially increase. The fact that the hysteresis phenomena shown in Figure 10 are most readily observed at lower pH, where the period of oscillation is shorter and where both process B and process C are more rapid, supports this view. Such behavior has also been observed in the Briggs–Rauscher[5] and Belousov–Zhabotinskii[18,19] systems.

With the exception of the above topological considerations, the results and discussion presented in this paper have been almost purely experimental. Although three overall processes (A), (B), and (C) have been suggested, no attempt has been made to construct a mechanism for this reaction. Before undertaking such a task, we feel that it is essential to understand the component processes and any other competing reactions. The kinetics of the chlorite–iodide reaction A have been thoroughly studied in batch conditons.[11,12] In contrast, almost nothing is known about the kinetics of the chlorite–iodine reaction B, which is apparently crucial in producing oscillations. Investigations of this system are now under way in this laboratory. Although much work has been done on the kinetics of the Dushman reaction (C), both its rate law[15] and its mechanism[15,20] remain subjects of some controversy. Finally, the role of chlorine dioxide, which is certainly present in significant amounts in the system at low pH, where oscillations are most prevalent, also remains to be established.

Given its central role in a new family of oscillatory reactions, the chlorite–iodide system is destined to be the subject of thorough study in the coming years. We emphasize here the importance of firmly establishing the kinetics of the component processes of this reaction, so that future mechanistic interpretations may have firm ground to rest upon.

Acknowledgment. This work was supported by a grant (No. CHE-7905911) from the National Science Foundation. We thank Professor Kenneth Kustin for many helpful discussions.

Registry No. ClO_2^-, 14998-27-7; I^-, 20461-54-5.

(18) De Kepper, P.; Boissonade, J. *J. Chem. Phys.* **1981**, *75*, 189–195.
(19) Maselko, J., unpublished results.
(20) Morgan, K. J.; Peard, M. G.; Cullis, C. F. *J. Chem. Soc.* **1951**, 1865–1867.

Diacetylene Monomers and Polymers with Chiral Substituents: Structure, Solid-State Polymerization, and Properties

Roxy B. Wilson,[†] Eileen N. Duesler,[†] David Y. Curtin,*[†] Iain C. Paul,*[†] Ray H. Baughman,*[‡] and Anthony F. Preziosi[‡]

Contribution from the Department of Chemistry, University of Illinois, Urbana, Illinois 61801, and Corporate Research Center, Allied Corporation, Morristown, New Jersey 07960.
Received December 22, 1980

Abstract: Two solid-state polymerizable monomer phases are obtained for the unresolved diacetylene having the chiral substituent group $-CH_2HC^*(CH_2CH_3)OCONHC_6H_5$. The crystals of the first phase (phase I) are orthorhombic, space group *Pbca*, with a = 45.982 (7), b = 10.879 (1), c = 9.603 (1) Å; there are eight molecules in the cell. A three-dimensional structure determination for phase I indicates chiral molecules which react by 1,4-addition polymerization of glide-related neighbors having opposite handedness to provide a regular backbone structure in which nearest-neighbor substituent groups have different chirality, but next-nearest-neighbor groups have the same chirality. The crystals of phase II are monoclinic, space group $P2_1/c$, with a = 5.181 (2), b = 36.629 (10), c = 6.827 (2) Å, β = 113.17 (2)°, and there are two diacetylene monomer molecules in the cell. Centrosymmetric diacetylene molecules present in the racemic phase II react by 1,4-addition polymerization with translation-related neighbors. Phase I polymerizes by solid solution formation to provide a polymer crystal, while phase II polymer is ordered only in the chain-axis projection. The polymerization reactions are interpreted using least motion and symmetry arguments. The structural work on phase I suggests that backbone strain provides the blue-shifted absorption spectra and excludes eximer emission from overlapping phenyls as the origin of strong fluorescence.

I. Introduction

The bis(phenylurethane) of 5,7-dodecadiyne-3,10-diol (UDD) provides reactive phases which polymerize in the solid state by 1,4-addition of the diacetylene groups. Several aspects of these compounds generate interest in the monomer and polymer phases. In contrast with other diacetylenes and polydiacetylenes for which structural information is available, the substituent groups on UDD are chiral. This substituent group chirality means that it is possible to isolate polymerizable crystalline phases consisting of either chiral molecules (R—C≡C—C≡C—R and S—C≡C—C≡C—S) or potentially centrosymmetric molecules (R—C≡C—C≡C—S), where R and S designate opposite handed forms of the substituent

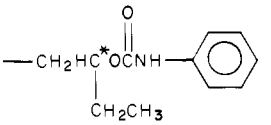

[†] University of Illinois.
[‡] Allied Corporation.

0002-7863/82/1504-0509$01.25/0